Journal of Molecular Liquids 389 (2023) 122931

Contents lists available at ScienceDirect

Journal of Molecular Liquids

journal homepage: www.elsevier.com/locate/molliq

# High-capacity adsorption of hexavalent chromium by a polyaniline-Ni(0) nanocomposite adsorbent: Expanding the Langmuir-Hinshelwood kinetic model

Luca Lohrentz [a], Madhumita Bhaumik [a], Hendrik G. Brink [a,*]

[a] Chemical Engineering Department, University of Pretoria, South Africa

ARTICLE INFO

*Keywords:*
Polyaniline nanotubes
Zero-valent nickel nanoparticles
Nanocomposite
Adsorption-coupled reduction
Langmuir kinetics

ABSTRACT

A nanocomposite of 2-napthalenesulfonic acid doped-polyaniline decorated with zero valent nickel nanoparticles (PANI-NSA@$Ni^0$), was considered for the removal of hexavalent chromium from synthetic effluent. Adsorption conditions (pH, dose) were optimised, and parameters necessary for the design of PANI-NSA@$Ni^0$-based adsorption equipment (adsorbent capacity, kinetic constants, etc.) were estimated from batch adsorption experiments. PANI-NSA@Ni0 successfully achieves total hexavalent chromium removal at a dose of 0.6 g/L, corresponding to a Cr(VI) loading of 333.3 mg/g, and when $2 < pH < 3$. The combined monolayer capacity of the adsorbent was found to be 820.5 mg/g, with equilibrium adsorption behaviour adequately described by a modified dual-site Langmuir isotherm model. The adsorption of Cr(VI) by PANI-NSA@$Ni^0$ was found to be largely unaffected by the presence of competing ions. Following adsorption, successful recovery of 95.5 % of adsorbed chromium was achieved by employing $HNO_3$ followed by NaOH as desorption agents, however this resulted in ≈ 88% loss in adsorption capacity for the subsequent cycle. After redeposition of $Ni^0$ on the desorbed material, the adsorbent's capacity was restored to 92% of the original capacity. An adsorption-coupled reduction mechanism, followed by the precipitation of Cr(OH)3, is believed to be the major mechanistic process responsible for Cr(VI) removal. Based on the proposed mechanism, a modified Langmuir-Hinshelwood adsorption-coupled reduction kinetic model was used to successfully describe the adsorption kinetics. The modified Langmuir-Hinshelwood adsorption-coupled reduction kinetic model produces rate constants which are independent of operating conditions such as initial pollutant concentration and adsorbent dose, and adequately describes the system's equilibrium using the same rate constants. Thermodynamic parameters calculated using the best fitting isotherm model and novel kinetic model were both in agreement, and revealed that the adsorption process proceeds spontaneously and endothermically, with an increase in randomness at the solid–liquid interface and potential changes in the structure of the adsorbent/adsorbate.

## 1. Introduction

The persistent nature of heavy metals, coupled with their tendency to bioaccumulate in organisms and cause chronic health problems, makes their removal from water systems a top engineering priority [1,2]. Chromium in its hexavalent form, i.e. Cr(VI), is a common constituent of tannery, electroplating, and dyeing effluent [3]. In an aquatic environment, Cr(VI) exhibits the highest mobility of all Cr species due to its superior water solubility [4]. Cr(VI) is estimated to be 500 times more toxic than its trivalent counterpart, with prolonged exposure leading to an increase in the incidence of cancer [1,5,6]. Furthermore, Cr(VI) is recognised as a potent neurotoxicant, and may cause toxicity by reducing the activity and efficiency of the immune system, supressing certain enzymes, and altering cell structures [4]. Current Cr(VI) removal techniques include methods such as reduction, precipitation, adsorption, membrane systems, ion-exchange, extraction, and electrolysis [3,7,8]. Of these techniques, adsorption has proven to be the most feasible [3]. The use of zero-valent metal nanoparticles (NPs) as adsorbents is of particular interest, since these particles are known to be highly effective adsorbents for heavy metal removal [9]. The adsorption properties of zero-valent metal NPs are believed to stem from the surface effect, small size effect, and quantum effect, which contribute to

* Corresponding author.
*E-mail address:* deon.brink@up.ac.za (H.G. Brink).

https://doi.org/10.1016/j.molliq.2023.122931
Received 8 May 2023; Received in revised form 6 August 2023; Accepted 24 August 2023
Available online 25 August 2023

increased specific surface area and reactivity, as well as their high reducing capacity [9]. Nanoparticle-based systems are however susceptible to aggregation and large pressure drops, which complicates their implementation in continuous flow systems such as fixed bed and mixed vessels [10]. To overcome the drawbacks of nanoparticles, they may be immobilised on polymer backbones to form a nanocomposite (NC) [9].

Of the various nanoparticle support matrices that exist, the organic polymer polyaniline (PANI) is an appealing choice due to its high specific surface area, low bulk-synthesis costs, and stability [11–13]. Furthermore, the conductivity of PANI allows for easier regeneration following adsorption [14]. These characteristics of PANI allow for the synthesis of high capacity, versatile adsorbents, such as the nanocomposite: 2-napthalenesulfonic acid doped PANI, decorated with zerovalent nickel nanoparticles (PANI-NSA@Ni0), whose structure is represented in Fig. 1. The use of such complex, hybrid adsorbents is twofold, firstly PANI's high number of amine and imine functional groups allow for higher interaction with organic pollutants [15,16]. In addition, the process of doping PANI results in charge transfer which enables it to interact electrostatically with ionic species such as heavy metals [17]. In this regard, PANI-NSA@$Ni^0$ has demonstrated its superior performance as an adsorbent for the heavy metal lead(II), exhibiting a high removal capacity of 414.6 mg/g at 25 °C, rapid sorption dynamics, and good selectivity [17]. However, despite numerous studies on PANI-based nanocomposites for the removal of Cr(VI), their capacities were found to be inadequate [18]. A PANI-based nanocomposite with superior Cr(VI) removal capacity is thus highly desirable, and PANI-NSA@$Ni^0$'s performance with lead(II) makes it a potential high-capacity adsorbent for Cr(VI) remediation.

Hence, the capacity of PANI-NSA@$Ni^0$ to remove Cr(VI) ions from synthetic effluent was investigated. PANI-NSA@$Ni^0$ was synthesised via a two-step, ex-situ synthesis procedure. Batch adsorption experiments were then conducted to evaluate the Cr(VI) adsorption performance of PANI-NSA@$Ni^0$. Optimal adsorption conditions (initial adsorbate concentration, pH, and adsorbent dose) were established, and thermodynamic parameters were estimated for the adsorption process. The influence of competing ions on chromium adsorption was investigated for binary and multi-component solutions. Recovery of chromium from the adsorbent was also investigated during desorption experiments. A mechanism for the adsorption process was then proposed by considering post-adsorption X-ray diffraction patterns and X-ray photoelectron spectroscopy spectra. Finally, a novel kinetic model based on the Langmuir kinetic model was derived and used to describe the adsorption kinetics and to determine the optimal adsorption time.

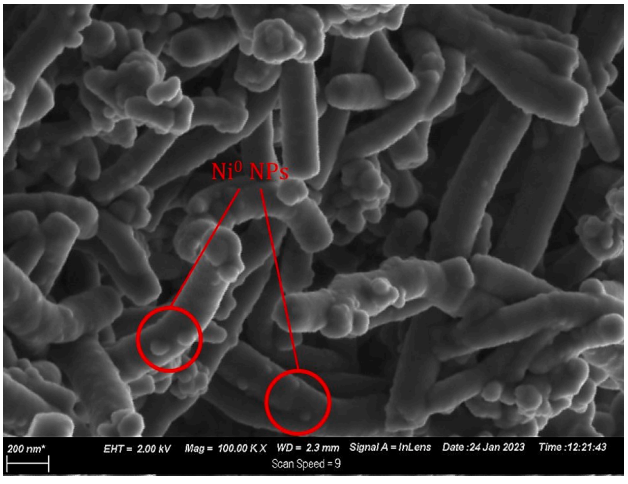


**Fig. 1.** High-resolution scanning electron micrograph of PANI-NSA@$Ni^0$ nanocomposite [12].

## 2. Materials and experimental methods

### 2.1. Materials

Aniline (99 %), ammonium persulfate, nickel (II) chloride hexahydrate ($NiCl_2{\cdot}6H_2O$), naphthalene-2-sulfonic acid, hydrazine hydrate (50 % – 60 %), ethylene glycol, and potassium dichromate ($K_2Cr_2O_7$) were obtained from Sigma-Aldrich, USA. All other reagents were also obtained from Sigma-Aldrich, USA. Deionised water was used in all experiments.

### 2.2. Methods

#### 2.2.1. PANI-NSA@$Ni^0$ synthesis

PANI-NSA@$Ni^0$ nanocomposite was synthesised by means of a two-step, ex-situ polymerization technique [12]. Firstly, 2-naphthalenesulfonic acid-doped polyaniline (PANI-NSA) was synthesised by means of rapid mixing chemical oxidative polymerisation, at 0–5 °C. Polymerisation of aniline in the presence of 2-napthalenesulfonic acid was achieved by employing ammonium persulfate as an oxidising agent. Reductive deposition of $Ni^0$ NPs onto the PANI-NSA support matrix was then performed at 60 °C in an ethylene glycol medium, using $NiCl_2{\cdot}6H_2O$ as the Ni source, and hydrazine hydrate as the reducing agent.

#### 2.2.2. Cr(VI) adsorption experiments

Batch adsorption experiments were performed in triplicate on synthetically formulated Cr(VI) effluent. A 1000 mg/L Cr(VI) stock solution was prepared by dissolving $K_2Cr_2O_7$ crystals in deionised water. The stock solution was subsequently diluted to the required concentration for each experiment. Where necessary, the initial solution pH was adjusted using 0.1 M NaOH and 0.1 M $HNO_3$, prior to nanocomposite addition. In all experiments, analysis of residual Cr(VI) concentrations was performed using a VWR UV-1600PC spectrophotometer, and the 1,5-Diphenylcarbazide method. Where applicable, total Cr concentrations were measured using an Atomic Absorptions Spectrometer (AAnalyst-400 AA, PerkinElmer).

The effect of the PANI-NSA@$Ni^0$ nanocomposite dose on the removal of Cr(VI) was investigated by treating 25 mL aliquots of a 200 mg/L Cr (VI) solution with variable doses of nanocomposite at the unadjusted solution pH (pH ≈ 4.53). For comparative purposes, identical experiments were conducted with bare $Ni^0$ NPs and PANI-NSA nanotubes (NTs). The experimental solutions were placed into a Labotec EcoBath 207 thermostatic shaker at 200 rpm and 25 °C for 24 h.

The effect of initial pH on Cr(VI) removal was also tested. Using 0.1 M NaOH and 0.1 M $HNO_3$, the pH of 25 mL aliquots of a 200 mg/L Cr(VI) solution were adjusted, such that each possessed a different pH (in the range of 2 – 11). To each aliquot, the optimal dose of PANI-NSA@$Ni^0$ (15 mg) was added, and the samples were placed into the thermostatic shaker at 200 rpm and 25 °C for 24 h.

Equilibrium adsorption isotherms were generated at 25 °C, 35 °C, and 45 °C using a thermostatic water bath shaker set at 200 rpm. The initial Cr(VI) concentration, $C_0$ (mg/L), was varied from 100 mg/L to 800 mg/L, and the solution pH was adjusted to an optimal pH of 3. To the 25 mL experimental solutions, 15 mg nanocomposite was added, and the equilibrium Cr(VI) concentration, $C_e$ (mg/L), was recorded after 24 h. The amount of Cr(VI) adsorbed onto the adsorbent at equilibrium, $q_e$ (mg/g), was calculated using Eq. (1):

$$q_e = (C_0 - C_e) \times \frac{V}{m} \tag{1}$$

with $V$ the experimental solution volume, and $m$ the adsorbent mass [12].

Initially, adsorption kinetics were studied at 25 °C, by contacting 500 mL of 10 mg/L, 25 mg/L, and 50 mg/L Cr(VI) solutions with 0.3 g nanocomposite in order to maintain the optimal dose. The solution pH

was again set at 3 prior to addition of the nanocomposite. Samples were analysed at predetermined time intervals to track the residual Cr(VI) concentration, $C_t$. The corresponding Cr(VI) loading onto the adsorbent as function of time, $q_t$, was calculated by employing Eq. (2) [12]:

$$q_t = (C_0 - C_t) \times \frac{V}{m} \quad (2)$$

The kinetic study was then extended to 35 °C and 45 °C, with all other parameters the same as in the 25 °C study.

The effect of competing ions on Cr(VI) adsorption was studied at 25 °C. Both anionic and cationic competing ions were considered, *viz.*, cobalt(II), zinc(II), copper(II), nitrate, and sulphate. Solutions of 25 mL, containing 200 mg/L Cr(VI) and 200 mg/L of the competing ion, were prepared. The solution pH was set at 3, and 15 mg of nanocomposite was added. The residual Cr(VI) concentration was then measured after 24 h.

The reusability of the nanocomposite was investigated by means of two subsequent adsorption–desorption cycles. For the adsorption stage, 100 mL of a 200 mg/L Cr(VI) solution was contacted with 60 mg of PANI-NSA@$Ni^0$ nanocomposite, maintaining the optimal dose. The residual total Cr concentrations were measured after 24 h. The spent nanocomposite was then desorbed using 50 mL of $HNO_3$, followed by 50 mL of NaOH. Varying desorbent concentrations (1 M, 0.5 M, and 0.1 M) were also considered in the experiment. For the regeneration of the desorbed material, the same Ni deposition method as described in section 2.2.1.

A generalised summary of the experimental procedure used for each experiment is provided in Fig. 2.

### 2.2.3. Characterization techniques

The crystallinity of the PANI-NSA@$Ni^0$ nanocomposite after adsorption was investigated using a PANalytical X'Pert Pro powder diffractometer with an X'Celerator detector. Using a Thermo ESCAlab 250Xi photoelectron spectrometer, the spent nanocomposite was also subjected to X-ray photoelectron spectroscopy (XPS) to identify the oxidation state of the $Ni^0$ NPs and adsorbed chromium species.

## 3. Results and discussion

### 3.1. Effect of adsorbent dose

The effect of the nanocomposite dose on the removal of Cr(VI) was investigated. The performance of PANI-NSA@$Ni^0$ nanocomposite was also compared to its constituents, PANI-NSA and bare $Ni^0$ NPs. Fig. 3 depicts the Cr(VI) removal efficiencies of PANI-NSA@$Ni^0$, PANI-NSA, and $Ni^0$ NPs. In general, the increase in removal efficiency observed when the dose is increased may be explained by considering the number of active adsorption sites [19,20]. As the dose is increased, more unspent adsorbent material with unoccupied adsorption sites is introduced into solution [12]. A greater amount of Cr(VI) may thus be adsorbed. Furthermore, PANI-NSA@$Ni^0$ displays an enhanced Cr(VI) removal efficiency in comparison to its constituents. At a PANI-NSA@$Ni^0$ dose of 25 mg no residual Cr(VI) was detected in solution after 24 h. In comparison, at the same dose of 25 mg, PANI-NSA and Ni0 NPs achieved 32.2 % (64.4 mg/g Cr(VI) loading) and 19.2 % (38.4 mg/g Cr(VI) loading) removal efficiencies, respectively. The higher removal efficiency of PANI-NSA@$Ni^0$ is attributed to its substantially higher specific surface area when compared to PANI-NSA and $Ni^0$ NPs [12]. The higher specific surface area of the nanocomposite arises from the inclusion of $Ni^0$ NPs, which possess a high specific surface area [21]. Furthermore, incorporation of the $Ni^0$ NPs in a nanocomposite stabilises, disperses,

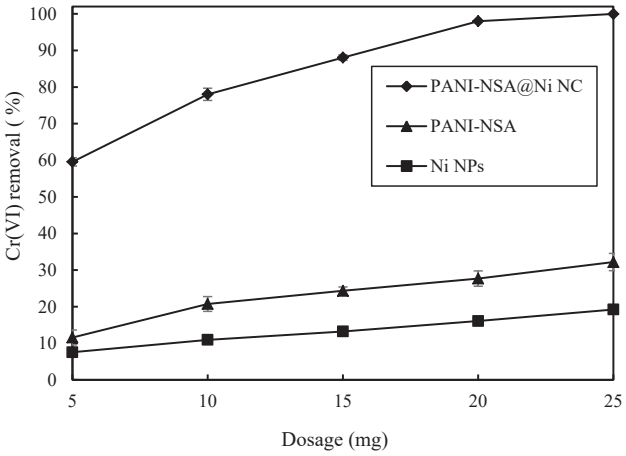


**Fig. 3.** Effect of the PANI-NSA@$Ni^0$ NC, PANI-NSA nanotube, and $Ni^0$ NP dose on the Cr(VI) removal efficiency (Initial conc.: 200 mg/L, pH: ~4.53, Temp.: 25 °C).

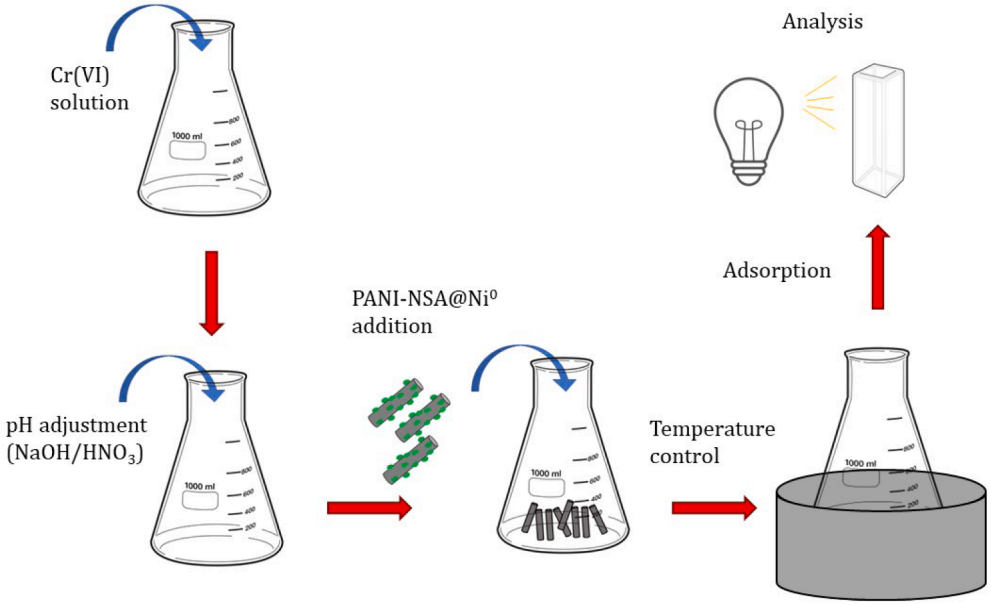


**Fig. 2.** Generalised experimental procedure for batch adsorption of Cr(VI) by PANI-NSA@$Ni^0$ nanocomposite.

and prevents their aggregation, which increases both their specific surface area and their reactivity [22].

### 3.2. Effect of initial pH

The initial solution pH, prior to the addition of the PANI-NSA@$Ni^0$ nanocomposite, was adjusted from pH = 2 to pH = 11. A nanocomposite dose of 15 mg/L was added to each aliquot, and the solution temperature was maintained at 25 °C. The residual Cr(VI) concentrations were then recorded after 24 h, with the results presented in Fig. 4. The final solution pH after adsorption was also recorded.

Higher Cr(VI) removal efficiencies were observed at lower pHs, with 100 % removal at pH = 2 and 98.6 % at pH = 3. At pHs lower than the nanocomposite's point-of-zero-charge ($pH_{PZC}$ = 4.4 [12]), the nanocomposite's surface becomes more positively charged. Electrostatic attraction forces between the nanocomposite and the Cr(VI) anions increase as the nanocomposite becomes more positively charged, thereby promoting adsorption [23]. The electrostatic interaction between Cr(VI) and PANI-NSA@$Ni^0$ at a pH of 3 is represented schematically in Fig. 5.

Furthermore, lower pHs favour the reduction of Cr(VI) to Cr(III) [24], which is described by Eqs. 3 and 4 under acidic conditions [25]. Conversely, at pHs above the $pH_{PZC}$, the nanocomposite assumes a negative surface charge. At high pHs, a decrease in adsorption efficiency may be attributed to electrostatic repulsive forces which counteract the van der Waals attraction forces, and an increase in competing $OH^-$ ions [11]. Under neutral and basic conditions, reduction of Cr(VI) to Cr(III) is given by Eq. 5, which exhibits a negative standard reduction potential (i.e. non-spontaneous reaction) [25]. Reduction of Cr(VI) under basic conditions is thus less favourable than under acidic conditions, which may also contribute to the decrease in Cr(VI) removal at higher pHs.

$$Cr_2O_7^- + 14H^+ + 6e^- \rightarrow 2Cr^{3+} + 7H_2O \; E^o = 1.232 \quad (3)$$

$$HCrO_4^- + 7H^+ + 3e^- \rightarrow Cr^{3+} + 4H_2O \; E^o = 1.350 \quad (4)$$

$$CrO_4^{2-} + 4H_2O + 3e^- \rightarrow Cr(OH)_3 + 5OH^- \; E^o = -0.1300 \quad (5)$$

For initial pHs < 9, an increase in the solution pH was observed following adsorption of Cr(VI), likely due to the consumption of protons during the reduction of Cr(VI) to Cr(III). At high pHs, adsorption of competing $OH^-$ ions may lead to the observed decrease in pH following adsorption.

### 3.3. Adsorption isotherms

Cr(VI) solutions of varying concentration (100 mg/L – 800 mg/L) were contacted with 0.6 g/L PANI-NSA@Ni0 nanocomposite, with the solution temperature maintained at 25 °C, 35 °C, and 45 °C respectively. Fig. 6. represents the amount of Cr(VI) adsorbed at equilibrium, $q_e$ (mg/g), as a function of the equilibrium concentration, $C_e$ (mg/L). To analyse the equilibrium data, the two most commonly used equilibrium isotherm models were employed, *viz.*, the Freundlich and single-site Langmuir isotherm models. In their non-linear forms, the single-site Langmuir and Freundlich isotherms are given by Eqs. (6) and (7), respectively [26]. Additionally, a modification of the dual-site Langmuir isotherm model [27], given by Eq. (8), was also investigated:

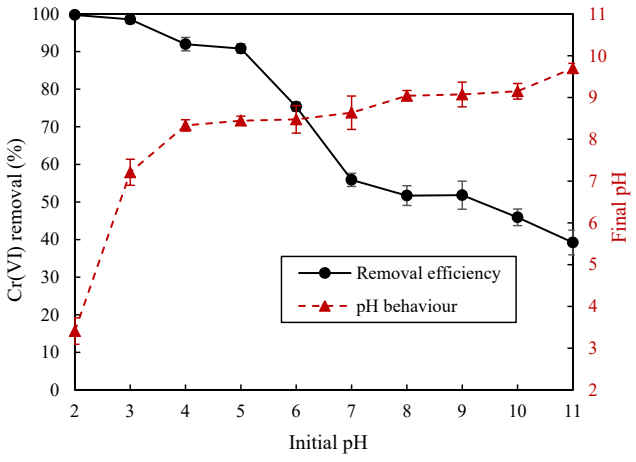


**Fig. 4.** Effect of initial solution pH on the Cr(VI) removal efficiency of PANI-NSA@$Ni^0$ NC (Initial conc.: 200 mg/L, NC dose: 0.6 g/L, Temp.: 25 °C).

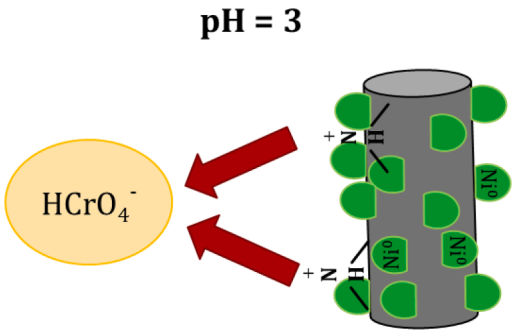


**Fig. 5.** Electrostatic interaction between PANI-NSA@$Ni^0$ nanocomposite and Cr(VI) molecules under acidic conditions (pH = 3).

$$q_e = \frac{q_{m1} K_{L1} C_e}{1 + K_{L1} C_e} \quad (6)$$

$$q_e = K_F C_e^{1/n} \quad (7)$$

$$q_e = \frac{q_{m1} K_{L1} C_e}{1 + K_{L1} C_e} + \frac{q_{m2} K_{L2} C_e}{1 + K_{L2} C_e} \quad (8)$$

with $q_{m1}$ and $q_{m2}$ the monolayer adsorption capacities of adsorption site 1 and 2 (mg/g), $K_{L1}$ and $K_{L2}$ the Langmuir isotherm/affinity constants for the respective sites (L/mg), and $K_F$ ((mg/g)(L/mg)$^{1/n}$) and $n$ the adsorption potential and strength constants of the Freundlich isotherm model. The high removal capacity observed at low equilibrium concentrations allude to an irreversible step in the adsorption process. Assuming adsorption site 2 in Eq. (8) adsorbs irreversibly, a very large value for $K_{L2}$ is anticipated. Thus, $K_{L2}C_e \gg 1$, and Eq. (8) simplifies to Eq. (9) as follows:

$$q_e = \frac{q_{m1} K_{L1} C_e}{1 + K_{L1} C_e} + q_{m2} \quad (9)$$

The isotherm model parameters for Eqs. (6), (7), and (9) were obtained by means of non-linear regression, with a summary of the fitting parameters provided in Table 1, and the full fitting parameters in Table S1.

The modified dual-site Langmuir isotherm model provided the best fit of the data, and generated the highest $R^2$ values compared to the single-site Langmuir and Freundlich isotherm models. The suitability of the modified dual-site Langmuir model alludes to the presence of two distinct adsorption sites, with adsorption at site 1 proceeding reversibly via formation of a monolayer, and adsorption at site 2 proceeding irreversibly. The capacity of the adsorbent was found to be insensitive to temperature, yet adsorption is marginally favoured at higher temperatures. The combined capacity of the adsorbent was estimated using the modified dual-site Langmuir isotherm model to be 820.5 mg/g. Table 2 compares the Cr(VI) adsorption capacity of PANI-NSA@$Ni^0$ with other PANI based adsorbents.

Evidently, PANI-NSA@$Ni^0$ nanocomposite exhibits a significantly higher affinity towards Cr(VI) in comparison to previously studied PANI-based adsorbents. The high capacity coupled with relatively rapid kinetics makes PANI-NSA@$Ni^0$ an extremely attractive choice for use in wastewater treatment processes.

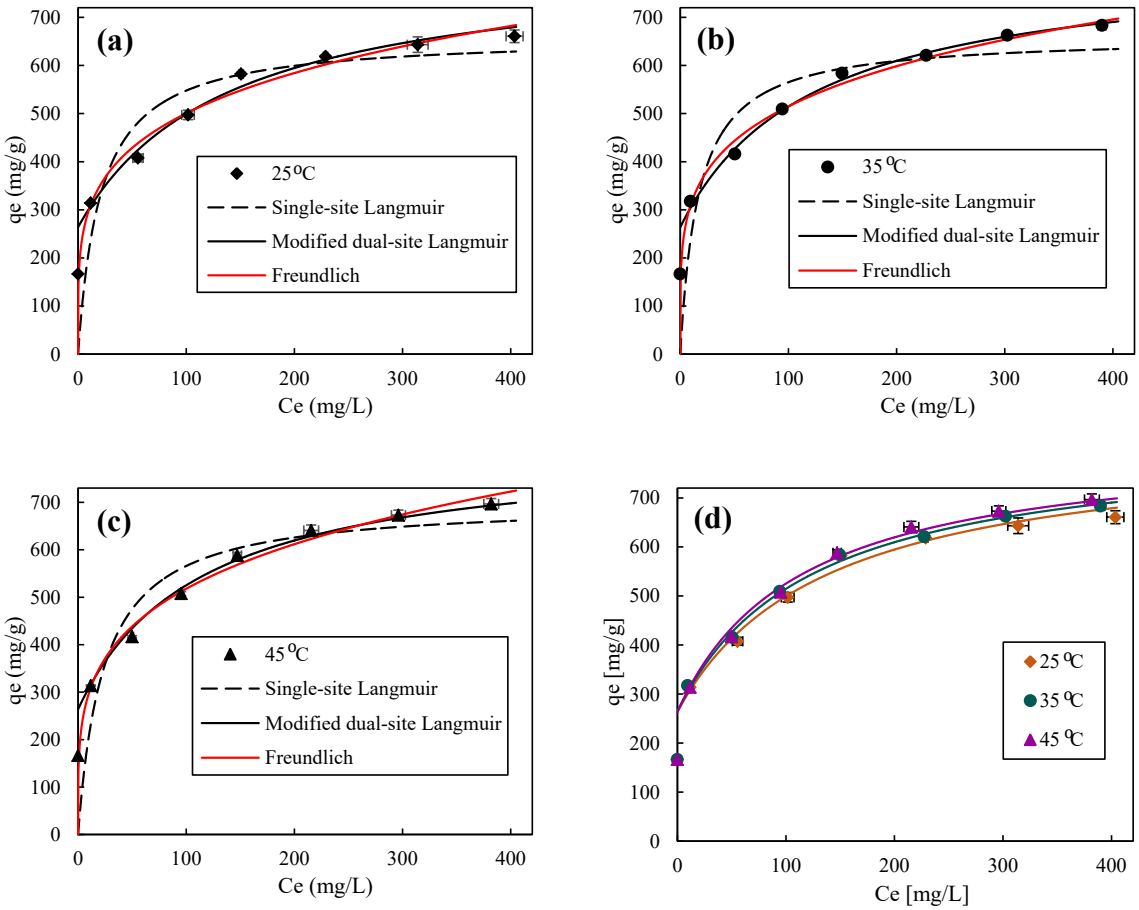


**Fig. 6.** (a - c) Equilibrium adsorption isotherms for removal of Cr(VI) by PANI-NSA@Ni$^0$ nanocomposite at 25 °C, 35 °C, and 45 °C, described by single-site Langmuir, modified dual-site Langmuir, and Freundlich isotherm models; and (d) comparison of adsorption isotherms across all temperatures using modified dual-site Langmuir isotherm model (Initial conc.: 100–800 mg/L, dose: 0.6 g/L and pH: 3.0).

### 3.4. Adsorption thermodynamics

The three commonly investigated thermodynamic parameters for an adsorption system are the standard Gibbs free energy change ($\Delta G^0$), entropy change ($\Delta S^0$) and change in enthalpy ($\Delta H^0$). Eqs. (10) and (11) were employed to obtain these thermodynamic parameters for the adsorption of Cr(VI) onto PANI-NSA@Ni$^0$ nanocomposite:

$$\Delta G^0 = -RT\ln(K_{eq}) \tag{10}$$

$$\ln(K_{eq}) = \frac{\Delta S^0}{R} - \frac{\Delta H^0}{RT} \tag{11}$$

where $R$ is the universal gas constant in (J/mol/K), $T$ (K) is the absolute temperature, and $K_{eq}$ is a non-dimensional equilibrium constant derived from an isotherm model [34]. The modified dual-site Langmuir isotherm equilibrium constants were non-dimensionalised by employing Eq. (12) as follows:

$$K_{eq} = K_{L1} \times M_w \times 10^3 \times \frac{C_s^o}{\gamma_s^o} \tag{12}$$

where $M_w$ is the molecular mass of the adsorbate, $C_s^o$ is the standard adsorbate concentration, and $\gamma_s^o$ is the standard adsorbate activity [34]. Both $C_s^o$ and $\gamma_s^o$ are frequently assumed to be unity [34]. The non-dimensionalised equilibrium constants are provided in Table 3.

The Van't Hoff plot used to obtain the above-mentioned thermodynamic parameters is presented in Fig. S1. Table 4 summarises the thermodynamic parameters for the adsorption system.

The positive value of $\Delta H^o$ indicates that the reversible pathway of the adsorption process is endothermic by nature, and that adsorption is favoured at higher temperatures. The positive value of $\Delta S^o$ alludes to an increase in randomness at the solid–liquid interface, and may also suggest structural changes in the adsorbate and the adsorbent [35]. Negative values for $\Delta G^o$ are indicative that the adsorption process proceeds spontaneously.

### 3.5. Effect of co-existing ions

Cr(VI) presents itself in numerous industrial effluents arising from processes such as electroplating, tanning, dyeing, printing, etc. [36]. In addition to Cr(VI), these industrial effluents frequently contain other metallic and non-metallic ions, which may affect the adsorption of chromium due to the competing ion effect [37]. Table 5 summarises the competing ions which are found in common effluents in addition to Cr (VI).

The effect of competing ions on the adsorption of Cr(VI) was thus studied in binary mode [42], as well as in a multicomponent mixture, with the results of the experiment represented in Fig. 7. In all experiments, the initial competing ion concentration and Cr(VI) concentration was set at 200 mg/L.

In the presence of Zn(II), Co(II), and Cu(II) cations the adsorption of Cr(VI) is unaffected, likely due to electrostatic repulsion between the positively charged nanocomposite and cations [43]. In contrast, the presence of nitrate and sulphate anions result in a decrease in the amount of Cr(VI) removed from solution, from 100 % to ~ 95 %. Electrostatic attraction between the positively charged PANI-NSA@Ni0 and the negatively charged anions may be responsible for the reduction in Cr

**Table 1**
Summary of the single-site Langmuir, modified dual-site Langmuir, and Freundlich isotherm model parameters for adsorption of Cr(VI) onto PANI-NSA@Ni$^0$ nanocomposite.

| Isotherm model | Temperature | | |
|---|---|---|---|
| | 25 °C | 35 °C | 45 °C |
| **Single-site Langmuir** | | | |
| Best-fit values | | | |
| $q_{m1}$ | 661.2 | 660.7 | 700.0 |
| $K_{L1}$ | 0.04830 | 0.05918 | 0.04222 |
| Goodness of fit | | | |
| $R2$ | 0.8437 | 0.8277 | 0.8722 |
| **Modified dual-site Langmuir** | | | |
| Best-fit values | | | |
| $q_{m1}$ | 556.6 [a] | | |
| $K_{L1}$ | 0.007324 | 0.008196 | 0.008851 |
| $q_{m2}$ | 263.9 [a] | | |
| Goodness of fit | | | |
| $R^2$ | 0.9796 | 0.9920 | 0.9918 |
| Global $R^2$ | 0.9881 | | |
| **Freundlich** | | | |
| Best-fit values | | | |
| $K_F$ | 179.0 | 189.7 | 171.3 |
| $n$ | 4.479 | 4.611 | 4.162 |
| Goodness of fit | | | |
| $R2$ | 0.9647 | 0.9820 | 0.9850 |

[a] Shared parameter for all data sets Units: $q_{m1}$, $q_{m2}$: mg/g, $K_{L1}$: L/mg, $K_F$: ((mg/g)(mg/L)$^{-1/n}$).

**Table 2**
Comparison of the Cr(VI) adsorption capacity of PANI-NSA@Ni$^0$ with other PANI based adsorbents.

| Adsorbent | $q_m$ (mg/g) | Optimum pH | Reference |
|---|---|---|---|
| PANI-HCL | 182.0 | 4.0 | [28] |
| PANI/PVA composite | 111.2 | 4.0 | [29] |
| Chitosan–grafted-polyaniline | 165.5 | 4.2 | [30] |
| PANI/γ-$Fe_2O_3$ | 196.0 | 2.0 | [31] |
| SA-PANI | 73.34 | 4.2 | [32] |
| PPy-PANI nanofibers | 227.0 | 2.0 | [33] |
| PANI-NSA@Ni$^0$ nanocomposite | 820.5 | 3.0 | Present study |

**Table 3**
Corrected equilibrium constants used in the calculation of the thermodynamic parameters for the removal of Cr(VI) by PANI-NSA@Ni$^0$ nanocomposite.

| Temperature (°C) | $K_{L1}$ | $K_{eq}$ |
|---|---|---|
| 25 | 0.007324 | 856.9 |
| 35 | 0.008196 | 958.9 |
| 45 | 0.008851 | 1036 |

Units: $K_{L1}$: L/mg.

**Table 4**
Thermodynamic parameters for the removal of Cr(VI) by PANI-NSA@Ni$^0$ nanocomposite.

| Temperature | $\Delta G$ ° | $\Delta H$ ° | $\Delta S$ ° | $R^2$ |
|---|---|---|---|---|
| 25 °C | −16.74 | 7.480 | 81.28 | 0.9920 |
| 35 °C | −17.59 | | | |
| 45 °C | −18.37 | | | |

Units: $\Delta H$ °: (kJ/mol), $\Delta S$ °: (J/mol/K), $\Delta G$ °: (kJ/mol).

**Table 5**
Composition of common industrial effluents.

| Effluent | Anions | Cations | References |
|---|---|---|---|
| Tannery | $SO_4^{2-}$, $Cl^-$, $S^{2-}$ | Cr(III), Cr(VI), Cd, Al, Zr | [38] |
| Electroplating | $SO_4^{2-}$ | Cu, Ni, Cr(III), Cr(VI), Sn, Pb, Ag, Au, Al, Zn | [39,40] |
| Dyeing | $Cl^-$, $NO_3^-$ | Co, Cu, Cr | [41] |

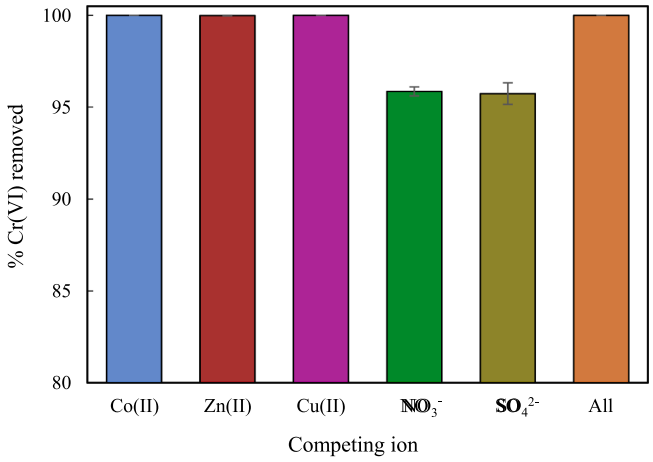


**Fig. 7.** The effect of competing ions on the adsorption of Cr(VI) onto PANI-NSA@NI$^0$ nanocomposite (Initial Cr(VI) conc.: 200 mg/L, competing ion conc.: 200 mg/L, pH: 3, NC dose: 0.6 g/L, Temp.: 25 °C).

(VI) removal [43]. In a multicomponent mixture, adsorption of Cr(VI) was found to be unaffected by the presence of the competing ions.

### 3.6. Investigation of Cr(VI) removal mechanism

The mechanism for Cr(VI) removal from water using PANI-NSA@Ni$^0$ nanocomposite was investigated by considering the results of the XPS survey on the nanocomposite before and after adsorption, presented in Fig. 8. The nanocomposite XRD patterns represented in Fig. S2. were also used to supplement the XPS survey results.

Appearance of characteristic Cr 2p peaks in the XPS scan confirm the presence of chromium on the adsorbent surface. High resolution spectrum of Cr 2p (Fig. 8a.) reveal peaks at 578.4 eV and 588.2 eV, which correspond to the 6 + oxidation state of chromium. In addition, Cr 2p peaks at 577 eV and 586.8 eV indicate attachment of trivalent chromium, Cr(III), on the adsorbent surface. Specifically, the observed Cr(III) peaks correspond to those of $Cr(OH)_3$. The simultaneous presence of both Cr(VI) and Cr(III) on the PANI-NSA@Ni0 nanocomposite surface suggests that Cr(VI) removal is achieved by means of an adsorption-coupled reduction mechanism, whereby a partial reduction of Cr(VI) to Cr(III) occurs during adsorption [44]. Comparison of the Ni 2p spectra before adsorption (Fig. 8b.) and after adsorption (Fig. 8c.) reveals disappearance of the Ni$^0$ peak following adsorption, which may suggest that Ni$^0$ functions as an electron donor, facilitating reduction of Cr(VI) to Cr(III). Disappearance of elemental Ni$^0$ is also confirmed by the XRD patterns. For the unspent nanocomposite (Fig. S2), sharp diffraction peaks at 2θ = 44.7°, 52.1°, and 76.7° are the signature peaks of (1 1 1), (2 0 0) and (2 2 0) crystal planes of metallic Ni$^0$ (JCPDS cards No. 65–0380). In addition, the XRD profile indicates peaks at 2θ = 23.5° and 27.0° corresponding to the (0 0 3) and (0 0 6) peaks for β-Ni(OH)$_2$ [45]. No such Ni-peaks presented in the XRD pattern for the spent adsorbent. The XRD pattern for the spent adsorbent reveals no evidence of crystalline structures, which may allude to morphological changes and a decrease in crystallinity of the nanocomposite following Cr(VI) adsorption. Participation of Ni$^0$ in the reduction of Cr(VI) is further

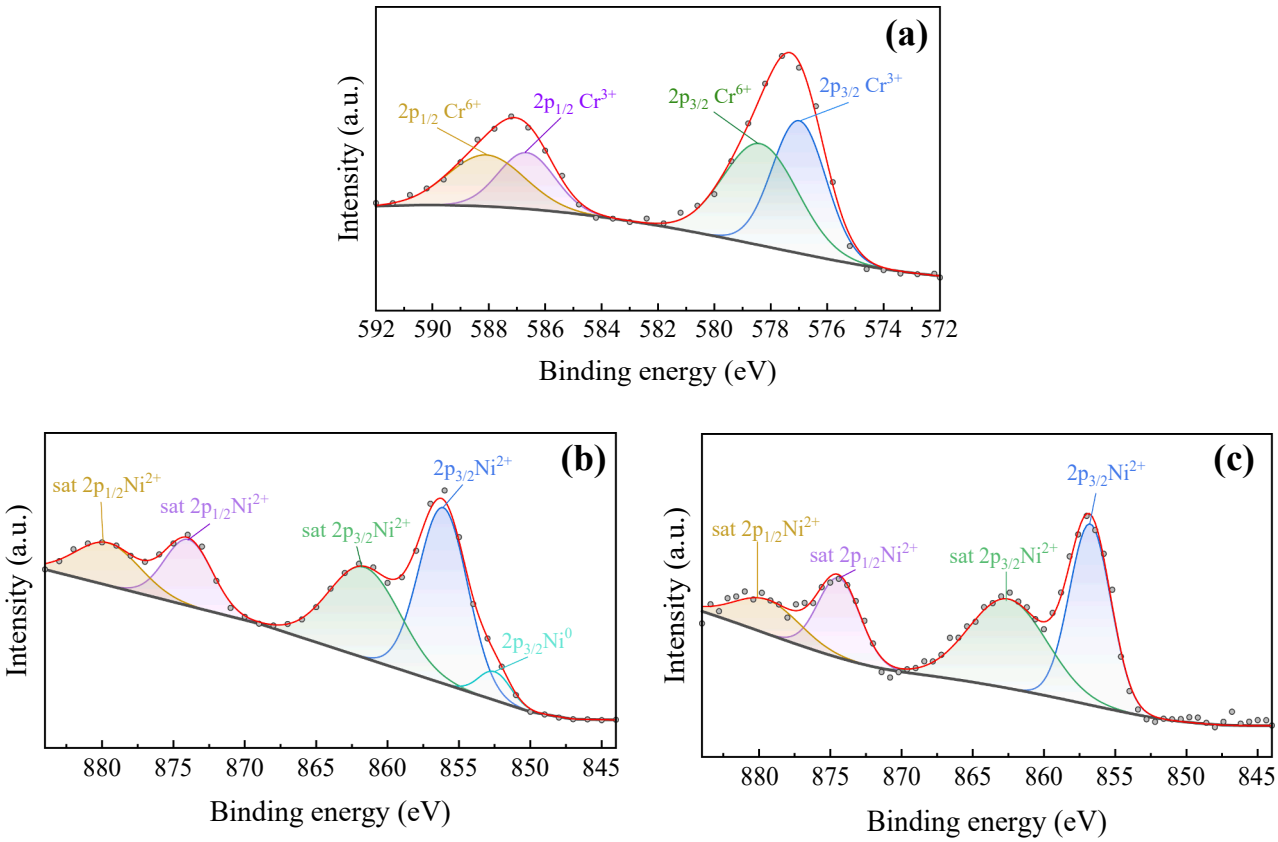


**Fig. 8.** (a) High resolution XPS spectra of Cr 2p after adsorption, (b) Ni 2p before adsorption of Cr(VI) by PANI-NSA@$Ni^0$ nanocomposite, and (c) Ni 2p after adsorption of Cr(VI).

corroborated by the standard reduction potential of $Ni^{2+}/Ni^0$ (-0.2800 V), which is significantly lower than that of $HCrO_4^-/Cr^{3+}$ (1.350 V) [9,25]. Hence, the superior suitability of the modified dual-site Langmuir isotherm model. The irreversible nature of the second Langmuir adsorption site is thus believed to represent the irreversible reduction of Cr(VI) to Cr(III) by $Ni^0$ nanoparticles.

Based on the results of the XPS survey, XRD patterns, as well as other observations from the study, the removal of Cr(VI) from water using PANI-NSA@$Ni^0$ nanocomposite is believed to occur via two major, parallel processes. In the first process, Cr(VI) in the form of $HCrO_4^-$ is adsorbed onto the surface of PANI-NSA@$Ni^0$ nanocomposite adsorbent, as follows:

$$\text{PANI-NSA@Ni}^0 + \text{HCrO}_4^-(\text{aq}) \leftrightarrow \text{PANI-NSA@Ni}^0 - \text{HCrO}_4^-(\text{ads}) \quad (13)$$

In the second process, irreversible reduction of some of the adsorbed Cr(VI) to Cr(III) then occurs as follows:

$$\text{PANI-NSA@Ni}^0 - \text{HCrO}_4^-(\text{ads}) \rightarrow \text{PANI-NSA@Ni}^{2+} - \text{Cr}^{3+}_{(\text{ads})} \quad (14)$$

As a final step, the Cr(III) present on the adsorbent surface precipitates and forms $Cr(OH)_3$, according to the following reaction:

$$\text{PANI-NSA@Ni}^{2+} - \text{Cr}^{3+}_{(\text{ads})} + 3\text{OH}^- \rightarrow \text{PANI-NSA@Ni}^{2+} - \text{Cr(OH)}_3 \quad (15)$$

Fig. 9. provides a graphical summary of the proposed mechanism for Cr(VI) removal from water using PANI-NSA@$Ni^0$ nanocomposite adsorbent.

### 3.7. Chromium recovery

Recovery of chromium from the nanocomposite is an important aspect to consider, as it enables reuse of these compounds in other industrial processes. Recovery of chromium from the adsorbent is also necessary, as metal-loaded adsorbents are toxic to humans and the

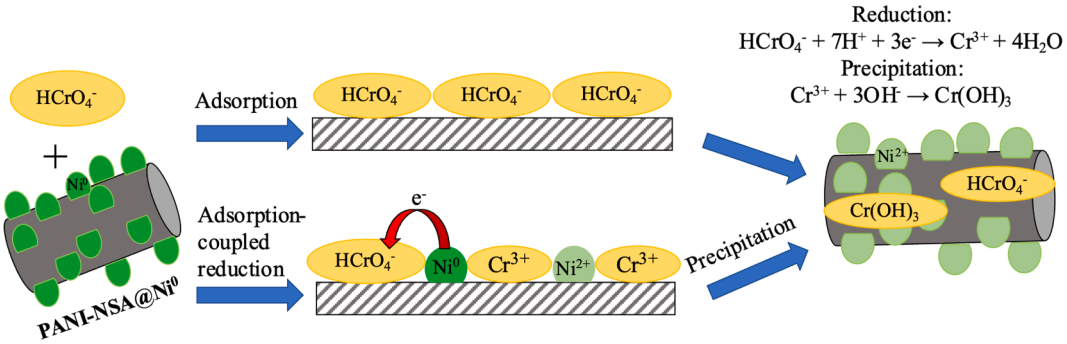


**Fig. 9.** Proposed mechanism for removal of Cr(VI) from water by PANI-NSA@$Ni^0$ nanocomposite adsorbent.

environment [46]. The recovery of Cr from spent PANI-NSA@$Ni^0$ nanocomposite is represented in Fig. 10.

No statistically significant difference in chromium recovery was observed between 1 M and 0.5 M desorption fluid, with 95.5 % of adsorbed chromium successfully recovered in the first cycle. The deficit is believed to arise from adsorbent losses during adsorption–desorption steps. In contrast, a decreased Cr recovery of 81.7 % was observed when 0.1 M desorption fluid was used, which may be due to the effect of pH on Cr(III) solubility [47]. Optimal desorption conditions therefore present when 0.5 M – 0.1 M is used.

Further studies are required to determine the exact optimum regenerant concentration. A significant decrease in adsorption capacity (~88 %) was observed in the subsequent adsorption cycle, which may be attributed to $Ni^0$ nanoparticles leaching into solution during nitric acid regeneration. Energy dispersive X-ray analysis (SEM-EDX) results contained in Table S2, confirm a reduction in nickel loading following desorption. The presence of nickel in the $HNO_3$ regenerant was also confirmed via Atomic Absorptions Spectrometer measurements. Additional regeneration steps are thus required if the original capacity is to be restored.

To improve the reusability of PANI-NSA@$Ni^0$ nanocomposite, the adsorbent was re-loaded with $Ni^0$ following the desorption process, with the $Ni^0$ loading also provided in Table S2. At $p < 0.05$, the regenerated nanocomposite showed no statistical difference in $Ni^0$ loading compared to the unspent nanocomposite, $t(15) = 0.4297$, $p = 0.6735$. It should however be noted that significant uncertainty exists with respect to the exact Ni loading, likely due to sensitivities in the synthesis process. To improve the nanocomposite's industrial feasibility, it would be necessary to identify and quantify such sensitivities.

Fig. 10(d) represents the performance of regenerated PANI-NSA@Ni0 nanocomposite. A drastic improvement in adsorption capacity was observed following $Ni^0$ re-deposition,with the adsorbent's capacity restored to 92 % of the original capacity.

### 3.8. Adsorption kinetics

The adsorption of Cr(VI) as a function of time is depicted in Fig. 11. The pseudo first-order (PFO), pseudo second-order (PSO) [48], and single-site Langmuir [49] kinetic equations given by Eqs. (16), (17), and (18) were employed to describe the adsorption kinetics:

$$q_t = q_e\left(1 - e^{-k_1 t}\right) \tag{16}$$

$$q_t = \frac{k_2 q_e^2 t}{1 + k_2 q_e t} \tag{17}$$

$$\frac{dq_t}{dt} = k_{ads} C_t \left(1 - \frac{q_t}{q_m}\right) - k_{des}\frac{q_t}{q_m} \tag{18}$$

where $k_1$ (L/min) is the PFO rate constant, $k_2$ (g/mg/min) is the PSO rate constant, $k_{ads}$ (L/g/min) and $k_{des}$ (mg/L/min) are the Langmuir adsorption and desorption rate constants. Application of the PFO and PSO models has become standard in adsorption studies [50], despite numerous drawbacks with respect to their engineering applications. Specifically, these models lack predictive capabilities as their parameters are complex functions of the experimental conditions such as initial adsorbate concentration [51]. Additionally, since these models are empirical, they lack physical meaning and thus cannot be used to investigate mass transfer mechanisms[52]. In contrast, the Langmuir kinetic model is able to produce concentration-independent kinetic parameters, whilst simultaneously predicting the equilibrium adsorption isotherms for some systems [53–55]. The parameters for PFO, PSO, and Langmuir kinetic models were obtained by means of non-linear

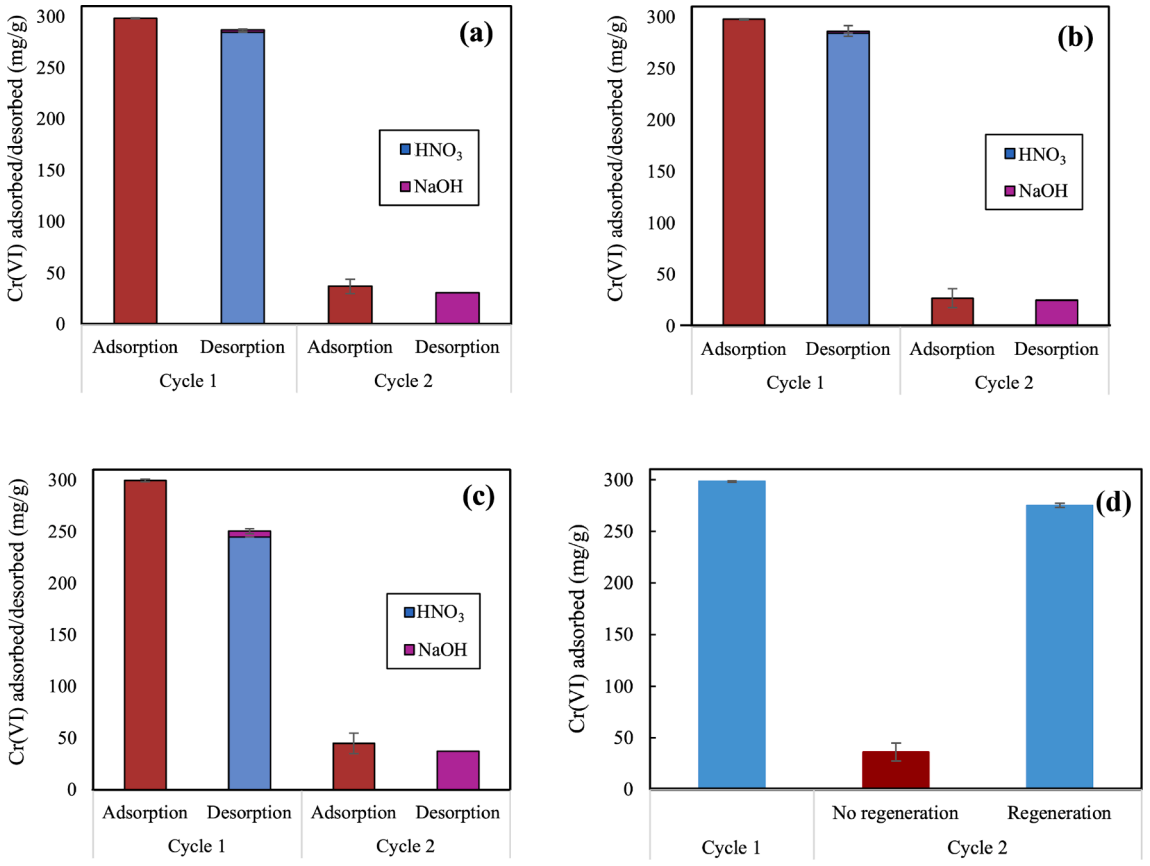


**Fig. 10.** Recovery of chromium from, and resusability of PANI-NSA@$Ni^0$ nanocomposite using (a) 1 M $HNO_3$ and 1 M NaOH, (b) 0.5 M $HNO_3$ and (c) 0.5 M NaOH, and 0.1 M $HNO_3$ and 0.1 M NaOH. (d) The reusability comparison of PANI-NSA@$Ni^0$ for non-regenerated and regenerated adsorbent after desorption.

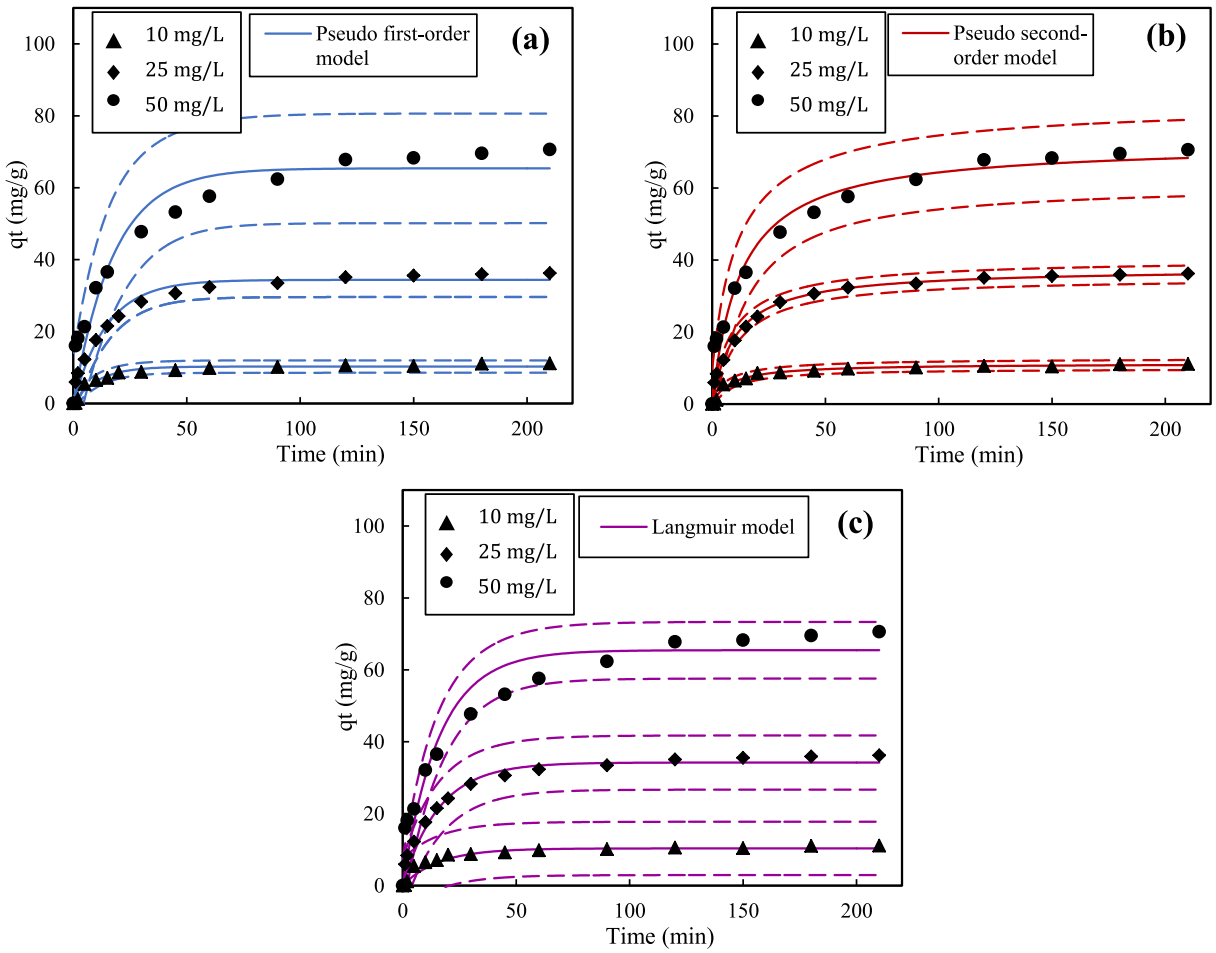


**Fig. 11.** (a) The effect of contact time on the adsorption of Cr(VI) by PANI-NSA@Ni$^0$ nanocomposite, described using the pseudo first-order kinetic model, (b) the pseudo second-order kinetic model and (c) the single-site Langmuir kinetic model. Dashed lines correspond to 95 % prediction intervals (NC dose: 0.6 g/L, Temp.: 25 °C, pH: 3.0).

regression fitting, and are presented in Table 6.

The PFO kinetic model was found to adequately describe the kinetics at lower concentrations, but becomes less suitable at higher concentrations. In contrast, the PSO model is capable of describing the adsorption kinetics across all concentration ranges. However, the dependence of the PFO and PSO model parameters on the experimental conditions is apparent and unpredictable. The Langmuir kinetic model successfully describes the adsorption at low concentrations, but similar to the PFO model, is unable to capture the system dynamics at higher concentrations. The Langmuir kinetic model's inability to fully describe the adsorption kinetics is likely due to the influence of Cr(VI) reduction on the observed kinetics. For such adsorption-reaction systems Langmuir-Hinshelwood kinetics are frequently employed [56]. However, the assumption of pseudo-equilibrium in these systems is necessary during formulation of rate expressions, which make the traditional Langmuir-Hinshelwood kinetic model unsuitable for many adsorption systems [56].

To address the shortcomings of the existing kinetic models, a Langmuir-based kinetic model was formulated, which accounts for the surface-reduction of Cr(VI) to Cr(III). The proposed model was built on the premise of the Langmuir-Hinshelwood kinetic model, but does not impose the requirement of pseudo-equilibrium conditions.

Consider the adsorption of a molecule of Cr(VI), predominantly in the form of $HCrO^{4-}$, onto a single PANI-NSA@Ni$^0$ adsorption site (S), which may be modelled as a reversible reaction, as follows:

$$\mathrm{Cr(VI)} + \mathrm{S} \leftrightharpoons \mathrm{Cr(VI)^*} \tag{19}$$

where Cr(VI)* signifies the adsorbed form of the Cr(VI) molecule. Adopting the Langmuir kinetic model, the rate of change of $C_t$ may be expressed as:

$$\frac{dC_t}{dt} = -k_{ads}C_t(1-\theta) + k_{des}\theta_{ads} \tag{20}$$

where θ is the total fraction of covered sites, and $\theta_{ads}$ is the fraction of sites covered by adsorbed Cr(VI). Distinction is made between total sites and adsorbed sites, since sites may also be occupied by reduced chromium species, i.e Cr(III). A site balance therefore yields:

$$\theta = \theta_{ads} + \theta_{red} \tag{21}$$

where $\theta_{red}$ is the fraction of sites occupied by Cr(III) species. The rate of change of θ can be expressed in terms of Eq. (20) and the monolayer adsorption capacity of PANI-NSA@Ni$^0$ as follows:

$$\frac{d\theta}{dt} = -\frac{1}{q_m} \times \frac{V}{m} \times \frac{dC_t}{dt} \tag{22}$$

An expression for $\theta_{red}$ was then derived by considering the combined redox reaction for the reduction of Cr(VI) to Cr(III) by Ni$^0$:

$$HCrO^{4-} + 7H^+ + \frac{3}{2}Ni^0 \rightarrow Cr^{3+} + 4H_2O + \frac{3}{2}Ni^{2+} \tag{23}$$

Assuming power-law kinetics, the rate of reduction of Cr(VI) was expressed as:

$$\frac{d[Cr^{3+}]}{dt} = k_{red}\theta_{ads}[Ni^0] \tag{24}$$

**Table 6**
Kinetics parameters for removal of Cr(VI) using PANI-NSA@$Ni^0$ nanocomposite.

| Kinetic model | Initial Concentration | | |
|---|---|---|---|
| | 10 mg/L | 25 mg/L | 50 mg/L |
| **Pseudo first-order** | | | |
| Best-fit values | | | |
| $q_e$ | 14.85 | 37.52 | 73.42 |
| $K_1$ | 0.2450 | 0.08385 | 0.08924 |
| Std. error | | | |
| $q_e$ | 0.4043 | 1.199 | 3.636 |
| $K_2$ | 0.04049 | 0.01153 | 0.02064 |
| 95% Confidence intervals | | | |
| $q_e$ | 13.98 to 15.72 | 34.93 to 40.12 | 65.50 to 81.34 |
| $K_2$ | 0.1575 to 0.3324 | 0.05894 to 0.1088 | 0.04427 to 0.1342 |
| Goodness of fit | | | |
| Degrees of freedom | 13 | 13 | 12 |
| $R2$ | 0.9354 | 0.9440 | 0.8657 |
| Absolute sum of squares | 20.64 | 128.0 | 1107 |
| Sy.x | 1.260 | 3.138 | 9.605 |
| Number of points analyzed | 15 | 15 | 14 |
| **Pseudo second-order** | | | |
| Best-fit values | | | |
| $q_e$ | 11.25 | 37.77 | 72.45 |
| $K_2$ | 0.01104 | 0.002554 | 0.001094 |
| Std. error | | | |
| $q_e$ | 0.2340 | 0.9461 | 3.406 |
| $K_2$ | 0.002473 | 0.0004408 | 0.0004646 |
| 95% Confidence intervals | | | |
| $q_e$ | 10.63 to 11.91 | 36.53 to 39.05 | 66.70 to 78.96 |
| $K_2$ | 0.008005 to 0.01533 | 0.002126 to 0.003079 | 0.0006810 to 0.001773 |
| Goodness of fit | | | |
| Degrees of freedom | 13 | 13 | 12 |
| $R2$ | 0.9790 | 0.9932 | 0.9675 |
| Absolute sum of squares | 4.566 | 14.19 | 234.9 |
| Sy.x | 0.5927 | 1.045 | 4.424 |
| Number of points analyzed | 15 | 15 | 14 |
| **Langmuir** | | | |
| Best-fit values | | | |
| $k_{ads}$ | 0.09235 [a] | | |
| $k_{des}$ | 4.840 [a] | | |
| $q_m$ | 820.5[a,b] | | |
| 95% Confidence intervals | | | |
| $k_{ads}$ | 0.07808 to 0.1066 | | |
| $k_{des}$ | 2.542 to 7.139 | | |
| Goodness of fit | | | |
| $R2$ | 0.9339 | 0.9704 | 0.9324 |
| Absolute sum of squares | 14.39 | 62.17 | 488.9 |
| Number of points analyzed | 15 | 15 | 14 |

[a] Shared parameter for all data sets.
[b] Obtained from isotherm data Units: $q_e$: mg/g; $q_{slow}$: mg/g; $k_1$, $k_{slow}$, $k_{fast}$: 1/min; $k_2$: g/mg.min; α: mg/g/min, $k_{ads}$: (L/g/min), $k_{des}$: $min^{-1}$.

with $[Cr^{3+}]$ the adsorbent Cr(III) loading (mmol/g), $[Ni^0]$ the zero-valent nickel nanoparticle loading (mmol/g), and $k_{red}$ the rate constant for the reduction reaction ($min^{-1}$). Similarly, the rate of change of $\theta_{red}$ is given by:

$$\frac{d\theta_{red}}{dt} = \frac{MW_{HCrO_4^-}}{q_m} \times \frac{d[Cr^{3+}]}{dt} \quad (25)$$

where $MW_{HCrO_4^-}$ is the molar mass of $HCrO_4^-$. Lastly, stoichiometry may be used to obtain an expression for the rate of consumption of $Ni^0$:

$$\frac{[dNi^0]}{dt} = -1.5\frac{d[Cr^{3+}]}{dt} \quad (26)$$

To increase the degrees of freedom, and the rate constants were expressed using the Arrhenius equation as follows:

$$k_{i,T} = k_{i,0}e^{\frac{E_{a,i}}{RT}} \quad (27)$$

with $k_{i,T}$ the reaction rate constant of the *i*th reaction at a temperature $T$, $k_{i,o}$ the frequency factor of the *i*th reaction, and $E_{a,i}$ the activation energy of the *i*th reaction.

The modified Langmuir-Hinshelwood adsorption-coupled reduction kinetic model is summarised in Table 7.

Using *Aquasim*, the novel model was fit to kinetic data at 25 °C, additional kinetic data at 35 °C and 45 °C, and the equilibrium isotherm data. Fig. 12 represents the adsorption kinetics as well as the equilibrium isotherms described using the modified Langmuir-Hinshelwood adsorption-coupled reduction kinetic model. Corresponding kinetic model parameters are presented in Table 8.

Using a bare minimum number of parameters, the modified Langmuir-Hinshelwood adsorption-coupled reduction kinetic model provided a good fit of the experimental data and achieved a global coefficient of determination of $R^2 = 0.9777$ for the kinetic data, and $R^2 = 0.9898$ for the isotherm data. Following non-dimensionalisation, the adsorption frequency factors, and activation energies were used to calculate the thermodynamic parameters of the system yielding $\Delta H^o = 11.50$ kJ/mol and $\Delta S^o = 90.76$ J/mol/K. The thermodynamic parameters are consistent with those predicted by the modified dual-site Langmuir isotherm model. Furthermore, the initial $Ni^0$ loading of 3.694 mmol/g, which translates to a ~ 22 wt% $Ni^0$ loading, is consistent with values estimated during nanocomposite synthesis.

The modified Langmuir-Hinshelwood model highlights the value in using Langmuir mechanistic models to describe adsorption kinetics and provides the compartment-independence needed to design batch and continuous adsorption equipment. Specifically, the model produces rate constants which are independent of operating conditions such as initial Cr(VI) concentration and nanocomposite dose.

## 4. Conclusions

PANI-NSA@$Ni^0$ was found to be a highly efficient adsorbent for the removal of hexavalent chromium from synthetic effluent. PANI-NSA@$Ni^0$'s enhanced efficiency allowed for total Cr(VI) removal, compared to its constituents, PANI-NSA and $Ni^0$ NPs, which achieved maximum removal efficiencies of 32.2 % and 19.2 % respectively. Optimum Cr(VI) removal was observed at a pH of 3, and a PANI-NSA@$Ni^0$ dose of 0.6 g/L. A modified dual-site Langmuir isotherm model was found to best describe the equilibrium adsorption behaviour and predicted a combined adsorbent capacity of 820.5 mg/g, one of the highest Cr(VI) adsorbent capacities reported in literature. The modified dual-

**Table 7**
Summary of the modified Langmuir-Hinshelwood adsorption-coupled reduction kinetic model for removal of Cr(VI) using PANI-NSA@$Ni^0$ nanocomposite.

| Unknown | Equation | Initial condition |
|---|---|---|
| $C_t$ | $\frac{dC_t}{dt} = -k_{ads}C_t(1-\theta) + k_{des}\theta_{ads}$ | Varies |
| $\theta$ | $\frac{d\theta}{dt} = -\frac{1}{q_m} \times \frac{V}{m} \times \frac{dC_t}{dt}$ | $\theta_0 = 0$ |
| $\theta_{red}$ | $\frac{d\theta_{red}}{dt} = \frac{MW_{HCrO_4^-}}{q_m} k_{red}\theta_{ads}[Ni^0]$ | $\theta_{red} = 0$ |
| $\theta_{ads}$ | $\theta_{ads} = \theta - \theta_{red}$ | N/A |
| $[Ni^0]$ | $\frac{[dNi^0]}{dt} = -1.5k_{red}\theta_{ads}[Ni^0]$ | $[Ni^0]_0 = f(q_{m2})^a$ |

[a] Dependent on PANI-NSA@$Ni^0$ nickel loading. Initial estimate based on $q_{m2}$.

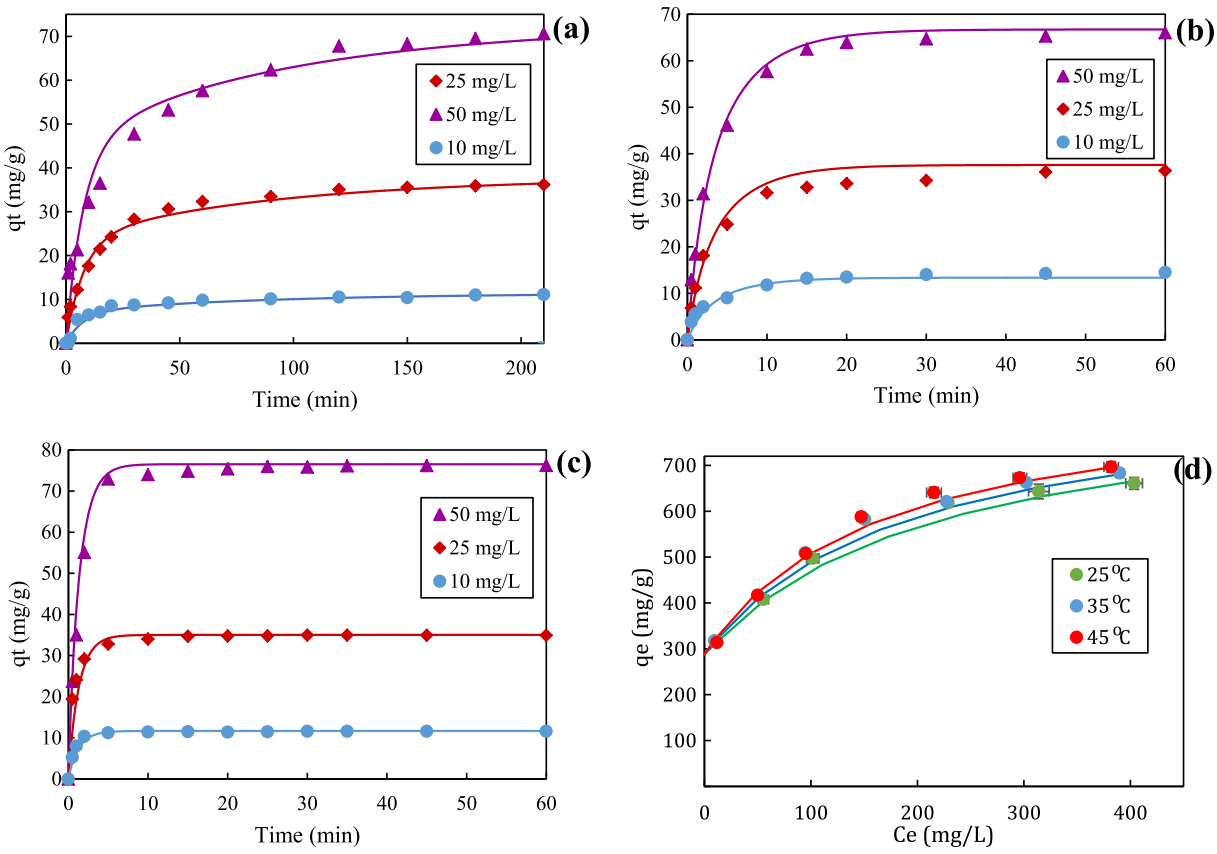


**Fig. 12.** The effect of contact time on the adsorption of Cr(VI) by PANI-NSA@$Ni^0$ nanocomposite at (a) 25 °C, (b) 35 °C, (c) and 45 °C, and (d) equilibrium isotherms described using the modified Langmuir-Hinshelwood adsorption-coupled reduction kinetic model (NC dose: 0.6 g/L, pH: 3.0).

**Table 8**
Modified Langmuir-Hinshelwood adsorption-coupled reduction kinetic model parameters for removal of Cr(VI) using PANI-NSA@$Ni^0$ nanocomposite.

| Parameter | Value | Units |
|---|---|---|
| $k_{des,o}$ | $4.188 \times 10^{12}$ | mg/(L·min) |
| $k_{ads,o}$ | $1.969 \times 10^{12}$ | $min^{-1}$ |
| $k_{red,o}$ | $1.033 \times 10^{29}$ | g/(mmol·min) |
| $E_{a,des}$ | 63.94 | kJ/mol |
| $E_{a,ads}$ | 75.44 | kJ/mol |
| $E_{a,red}$ | 176.9 | kJ/mol |
| $q_m$ | 871.4 | mg/g |
| $[Ni^0]_0$ | 3.694 | mmol/g |

site Langmuir isotherm model alludes to the presence of both an irreversible and reversible process during the adsorption of Cr(VI), with the irreversible process being the reduction of Cr(VI) to Cr(III) by highly reactive $Ni^0$ nanoparticles. PANI-NSA@$Ni^0$ was also found to selectively adsorb Cr(VI) in the presence of both cationic and anionic competing ions, with $NO_3^-$ and $SO_4^{2-}$ anions only slightly reducing the Cr(VI) removal efficiency. Recovery of chromium from spent PANI-NSA@$Ni^0$ was also successfully demonstrated, with 95.5 % of loaded chromium recovered from the nanocomposite after treatment with 0.5 M $HNO_3$ followed by 0.5 M NaOH, however this resulted in ≈ 88% loss in adsorption capacity for the subsequent cycle. The adsorbent's capacity was then successfully restored to 92% of the original capacity by redepositing $Ni^0$ on the desorbed material. Mechanistically, adsorption-coupled reduction and subsequent precipitation appear to be the major processes resulting in Cr (VI) removal using PANI-NSA@$Ni^0$. The adsorption-coupled reduction mechanism was confirmed by kinetic studies, where a modified Langmuir-Hinshelwood adsorption-coupled reduction kinetic model was successfully used to describe both the adsorption kinetics, as well as the equilibrium isotherms using the same parameters. The modified Langmuir-Hinshelwood adsorption-coupled reduction kinetic model provides the compartment-independence required to design any batch or continuous adsorption system, and thus should be preferred over traditional empirical adsorption kinetic models. Thermodynamic analysis during equilibrium and kinetic studies revealed that adsorption onto PANI-NSA@$Ni^0$ surface sites proceeds spontaneously and is weakly endothermic, with an increase in randomness at the adsorption interface and potential changes in the structure of the adsorbent/adsorbate.

## CRediT authorship contribution statement

**Luca Lohrentz:** Conceptualization, Investigation, Methodology, Data curation, Validation, Writing – original draft, Formal analysis, Writing – review & editing. **Madhumita Bhaumik:** Conceptualization, Methodology, Writing – original draft, Writing – review & editing, Formal analysis, Supervision. **Hendrik G. Brink:** Data curation, Software, Formal analysis, Writing – original draft, Writing – review & editing, Funding acquisition, Resources, Supervision.

## Declaration of Competing Interest

The authors declare that they have no known competing financial interests or personal relationships that could have appeared to influence the work reported in this paper.

## Data availability

Data will be made available on request.

## Acknowledgement

This work is based on the research supported in part by the National Research Foundation of South Africa (Grant Numbers: 120321, 132732, 145848, CSRP220420402).

## Appendix A. Supplementary data

Supplementary data to this article can be found online at https://doi.org/10.1016/j.molliq.2023.122931.

## References

[1] A. Linos, A. Petralias, C.A. Christophi, E. Christoforidou, P. Kouroutou, M. Stoltidis, A. Veloudaki, E. Tzala, K.C. Makris, M.R. Karagas, Oral ingestion of hexavalent chromium through drinking water and cancer mortality in an industrial area of Greece-an ecological study, Environ. Health 10 (2011) 1–8.
[2] S. Tabrez, T.A. Zughaibi, M. Javed, Bioaccumulation of heavy metals and their toxicity assessment in Mystus species, Saudi, J. Biol. Sci. 28 (2) (2021) 1459–1464.
[3] S.S. Baral, S.N. Das, P. Rath, Hexavalent chromium removal from aqueous solution by adsorption on treated sawdust, Biochem. Eng. J. 31 (3) (2006) 216–222.
[4] P. Sharma, S.P. Singh, S.K. Parakh, Y.W. Tong, Health hazards of hexavalent chromium (Cr (VI)) and its microbial reduction, Bioengineered. 13 (3) (2022) 4923–4938.
[5] R.A. Anderson, Chromium as an essential nutrient for humans, Regul. Toxicol. Pharm. 26 (1) (1997) S35–S41.
[6] N. Itankar, Y. Patil, Management of hexavalent chromium from industrial waste using low-cost waste biomass, Procedia Soc. Behav. Sci. 133 (2014) 219–224.
[7] B.A.M. Al-Rashdi, D.J. Johnson, N. Hilal, Removal of heavy metal ions by nanofiltration, Desalination 315 (2013) 2–17.
[8] D. Pradhan, L.B. Sukla, M. Sawyer, P.K.S.M. Rahman, Recent bioreduction of hexavalent chromium in wastewater treatment: A review, J. Ind. Eng. Chem. 55 (2017) 1–20.
[9] J. Yang, B. Hou, J. Wang, B. Tian, J. Bi, N. Wang, X. Li, X. Huang, Nanomaterials for the removal of heavy metals from wastewater, Nanomaterials 9 (2019) 424.
[10] M. Hua, S. Zhang, B. Pan, W. Zhang, L. Lv, Q. Zhang, Heavy metal removal from water/wastewater by nanosized metal oxides: a review, J. Hazard. Mater. 211 (2012) 317–331.
[11] M. Bhaumik, A. Maity, V.V. Srinivasu, M.S. Onyango, Enhanced removal of Cr (VI) from aqueous solution using polypyrrole/Fe3O4 magnetic nanocomposite, J. Hazard. Mater. 190 (1-3) (2011) 381–390.
[12] M. Bhaumik, A. Maity, H.G. Brink, Zero valent nickel nanoparticles decorated polyaniline nanotubes for the efficient removal of Pb (II) from aqueous solution: Synthesis, characterization and mechanism investigation, Chem. Eng. J. 417 (2021), 127910.
[13] G. Zhao, X. Huang, Z. Tang, Q. Huang, F. Niu, X. Wang, Polymer-based nanocomposites for heavy metal ions removal from aqueous solution: a review, Polym. Chem. 9 (26) (2018) 3562–3582.
[14] A. Muhammad, A.-H.-A. Shah, S. Bilal, G. Rahman, Basic Blue dye adsorption from water using Polyaniline/Magnetite (Fe3O4) composites: Kinetic and thermodynamic aspects, Materials. 12 (2019) 1764.
[15] J. Shen, S. Shahid, I. Amura, A. Sarihan, M. Tian, E.A.C. Emanuelsson, Enhanced adsorption of cationic and anionic dyes from aqueous solutions by polyacid doped polyaniline, Synth. Met. 245 (2018) 151–159.
[16] B. Saha, A. Debnath, B. Saha, Fabrication of PANI@Fe–Mn–Zr hybrid material and assessments in sono-assisted adsorption of methyl red dye: Uptake performance and response surface optimization, J. Indian Chem. Soc. 99 (9) (2022) 100635.
[17] M. Bhaumik, A. Maity, H.G. Brink, Zero valent nickel nanoparticles decorated polyaniline nanotubes for the efficient removal of Pb(II) from aqueous solution: Synthesis, characterization and mechanism investigation, Chem. Eng. J. 417 (2021), 127910, https://doi.org/10.1016/j.cej.2020.127910.
[18] Y. Jiang, Z. Liu, G. Zeng, Y. Liu, B. Shao, Z. Li, Y. Liu, W. Zhang, Q. He, Polyaniline-based adsorbents for removal of hexavalent chromium from aqueous solution: a mini review, Environ. Sci. Pollut. Res. Int. 25 (2018) 6158–6174, https://doi.org/10.1007/s11356-017-1188-3.
[19] V.T.P. Vinod, R.B. Sashidhar, B. Sreedhar, Biosorption of nickel and total chromium from aqueous solution by gum kondagogu (Cochlospermum gossypium): A carbohydrate biopolymer, J. Hazard. Mater. 178 (1-3) (2010) 851–860.
[20] R. Beksissa, B. Tekola, T. Ayala, B. Dame, Investigation of the adsorption performance of acid treated lignite coal for Cr (VI) removal from aqueous solution, Environmental Challenges. 4 (2021), 100091.
[21] P. Xu, G.M. Zeng, D.L. Huang, C.L. Feng, S. Hu, M.H. Zhao, C. Lai, Z. Wei, C. Huang, G.X. Xie, Z.F. Liu, Use of iron oxide nanomaterials in wastewater treatment: a review, Sci. Total Environ. 424 (2012) 1–10.
[22] X. Zhang, S. Lin, Z. Chen, M. Megharaj, R. Naidu, Kaolinite-supported nanoscale zero-valent iron for removal of Pb2+ from aqueous solution: reactivity, characterization and mechanism, Water Res. 45 (2011) 3481–3488.
[23] M. Alsuhybani, A. Alshahrani, M. Algamdi, A.A. Al-Kahtani, A.A. Alqadami, Highly efficient removal of Pb (II) from aqueous systems using a new nanocomposite: Adsorption, isotherm, kinetic and mechanism studies, J. Mol. Liq. 301 (2020), 112393.
[24] L. Anah, N. Astrini, Influence of pH on Cr(VI) ions removal from aqueous solutions using carboxymethyl cellulose-based hydrogel as adsorbent, IOP Conf. Ser.: Earth Environ. Sci. 60 (2017) 012010.
[25] P. Vanysek, Electrochemical series, CRC Handbook of Chemistry and Physics. 87 (1998).
[26] O.P. Murphy, M. Vashishtha, P. Palanisamy, K.V. Kumar, A Review on the Adsorption Isotherms and Design Calculations for the Optimization of Adsorbent Mass and Contact Time, ACS Omega 8 (20) (2023) 17407–17430.
[27] I. Langmuir, The adsorption of gases on plane surfaces of glass, mica and platinum, J. Am. Chem. Soc. 40 (1918) 1361–1403, https://doi.org/10.1021/ja02242a004.
[28] J. Wang, K. Zhang, L. Zhao, Sono-assisted synthesis of nanostructured polyaniline for adsorption of aqueous Cr (VI): effect of protonic acids, Chem. Eng. J. 239 (2014) 123–131.
[29] R. Karthik, S. Meenakshi, Adsorption study on removal of Cr (VI) ions by polyaniline composite, Desalination, Water Treat. 54 (11) (2015) 3083–3093.
[30] R. Karthik, S. Meenakshi, Facile synthesis of cross linked-chitosan–grafted-polyaniline composite and its Cr (VI) uptake studies, Int. J. Biol. Macromol. 67 (2014) 210–219.
[31] A.E. Chávez-Guajardo, J.C. Medina-Llamas, L. Maqueira, C.A.S. Andrade, K.G. B. Alves, C.P. de Melo, Efficient removal of Cr (VI) and Cu (II) ions from aqueous media by use of polypyrrole/maghemite and polyaniline/maghemite magnetic nanocomposites, Chem. Eng. J. 281 (2015) 826–836.
[32] R. Karthik, S. Meenakshi, Removal of Cr (VI) ions by adsorption onto sodium alginate-polyaniline nanofibers, Int. J. Biol. Macromol. 72 (2015) 711–717.
[33] M. Bhaumik, S. Agarwal, V.K. Gupta, A. Maity, Enhanced removal of Cr (VI) from aqueous solutions using polypyrrole wrapped oxidized MWCNTs nanocomposites adsorbent, J. Colloid Interface Sci. 470 (2016) 257–267.
[34] H.N. Tran, E.C. Lima, R.-S. Juang, J.-C. Bollinger, H.-P. Chao, Thermodynamic parameters of liquid–phase adsorption process calculated from different equilibrium constants related to adsorption isotherms: A comparison study, J. Environ. Chem. Eng. 9 (6) (2021) 106674.
[35] P. Saha, S. Chowdhury, Insight into adsorption thermodynamics, Thermodynamics. 16 (2011) 349–364.
[36] S. Mitra, A. Sarkar, S. Sen, Removal of chromium from industrial effluents using nanotechnology: a review, Nanotechnology for, Environ. Eng. 2 (2017) 1–14.
[37] S. Kong, D.R. Yonge, D.L. Johnstone, J.N. Petersen, T.M. Brouns, Competing ion effect on chromium adsorption with fresh and starved subsurface bacterial consortium, Biotechnol. Lett 15 (1) (1993) 87–92.
[38] M. Bosnic, J. Buljan, R.P. Daniels, Pollutants in tannery effluents, United Nations Industrial Development, Organization 26 (2000).
[39] H.S.S. Chiu, K.L. Tsang, R.M.L. Lee, Treatment of electroplating wastes, J. Inst. Water Pollut. Control. 86 (1987) 12–19.
[40] I. Dobrevsky, M. Dimova-Todorova, T. Panayotova, Electroplating rinse waste water treatment by ion exchange, Desalination 108 (1-3) (1997) 277–280.
[41] D.A. Yaseen, M. Scholz, Textile dye wastewater characteristics and constituents of synthetic effluents: a critical review, Int. J. Environ. Sci. Technol. 16 (2019) 1193–1226.
[42] B. Xiao, K.M. Thomas, Competitive adsorption of aqueous metal ions on an oxidized nanoporous activated carbon, Langmuir 20 (11) (2004) 4566–4578.
[43] J.R. Guarín-Romero, P. Rodríguez-Estupiñán, L. Giraldo, J.C. Moreno-Piraján, Simple and competitive adsorption study of nickel (II) and chromium (III) on the surface of the brown algae Durvillaea antarctica biomass, ACS Omega 4 (19) (2019) 18147–18158.
[44] A.T. Vo, V.P. Nguyen, A. Ouakouak, A. Nieva, B.T. Doma Jr, H.N. Tran, H.-P. Chao, Efficient removal of Cr (VI) from water by biochar and activated carbon prepared through hydrothermal carbonization and pyrolysis: adsorption-coupled reduction mechanism, Water (Basel). 11 (2019) 1164.
[45] H.W. Park, J.S. Chae, S.M. Park, K.B. Kim, K.C. Roh, Nickel-based layered double hydroxide from guest vanadium oxide anions, Met. Mater. Int. 19 (2013) 887–894, https://doi.org/10.1007/s12540-013-4034-2.
[46] S. Lata, P.K. Singh, S.R. Samadder, Regeneration of adsorbents and recovery of heavy metals: a review, Int. J. Environ. Sci. Technol. 12 (4) (2015) 1461–1478.
[47] D. Rai, B.M. Sass, D.A. Moore, Chromium (III) hydrolysis constants and solubility of chromium (III) hydroxide, Inorg. Chem. 26 (3) (1987) 345–349.
[48] L. Largitte, R. Pasquier, A review of the kinetics adsorption models and their application to the adsorption of lead by an activated carbon, Chem. Eng. Res. Des. 109 (2016) 495–504.
[49] K.L. Muedi, H.G. Brink, V. Masindi, J.P. Maree, Effective removal of arsenate from wastewater using aluminium enriched ferric oxide-hydroxide recovered from authentic acid mine drainage, J. Hazard. Mater. 414 (2021), 125491.
[50] M. Hubbe, S. Azizian, S. Douven, Implications of apparent pseudo-second-order adsorption kinetics onto cellulosic materials: A review, BioResources 14 (3) (2019) 7582–7626.
[51] J.C. Bullen, S. Saleesongsom, K. Gallagher, D.J. Weiss, A revised pseudo-second-order kinetic model for adsorption, sensitive to changes in adsorbate and adsorbent concentrations, Langmuir 37 (10) (2021) 3189–3201.
[52] J. Wang, X. Guo, Adsorption kinetic models: Physical meanings, applications, and solving methods, J. Hazard. Mater. 390 (2020), 122156.
[53] Y. Li, B. Gao, T. Wu, B. Wang, X. Li, Adsorption properties of aluminum magnesium mixed hydroxide for the model anionic dye Reactive Brilliant Red K-2BP, J. Hazard. Mater. 164 (2-3) (2009) 1098–1104.

[54] S. Salvestrini, Analysis of the Langmuir rate equation in its differential and integrated form for adsorption processes and a comparison with the pseudo first and pseudo second order models, React. Kinet. Mech. Catal. 123 (2018) 455–472.
[55] S. Azizian, Kinetic models of sorption: a theoretical analysis, J. Colloid Interface Sci. 276 (1) (2004) 47–52.
[56] H.S. Fogler, Elements of chemical reaction engineering, Pearson Boston, 2020.